Materials Characterization 203 (2023) 113097

Contents lists available at ScienceDirect

Materials Characterization

journal homepage: www.elsevier.com/locate/matchar

Evaluation of structural and electrical properties of multicomponent spinel oxide thin films deposited via spray pyrolysis technique

B. Kamecki [a,b,*], J. Karczewski [a], G. Cempura [c], P. Jasiński [b], S. Molin [b]

[a] Advanced Materials Center, Faculty of Applied Physics and Mathematics, Gdańsk University of Technology, ul. G. Narutowicza 11/12, 80-233 Gdańsk, Poland
[b] Advanced Materials Center, Faculty of Electronics, Telecommunications and Informatics, Gdańsk University of Technology, ul. G. Narutowicza 11/12, 80-233 Gdańsk, Poland
[c] Faculty of Metals Engineering and Industrial Computer Science, International Centre for Electron Microscopy, AGH University of Science and Technology, al. A. Mickiewicza, Kraków, Poland

ARTICLE INFO

Keywords:
Thin films
Deposition
Crystallisation
Grain growth
Spray pyrolysis

ABSTRACT

This work reports the preparation of $(Mn,Co,Fe,Ni,Cr)_3O_4$ high-entropy spinel oxide in the form of a ~ 500 nm thin film utilising a facile spray pyrolysis technique. The structural and electrical properties of the layers were characterised after exposure to temperatures in the range of 400–900 °C. The as-deposited layers were amorphous, and crystallised upon heat treatment at 500 °C. Microstructural analyses proved a homogeneous elemental distribution and the desired Fd-3 m cubic spinel structure. Electrical conductivity measurements indicated a dependence on the processing temperature, with the highest electrical conductivity values (~3 S cm^{-1} at 700 °C) obtained for layers heat-treated at 700 °C. The spray pyrolysis technique seems to be well suited to fabricating and exploring spinel-based high-entropy oxides synthesized as thin films, and to studying new compositions containing transition metal cations.

1. Introduction

The idea of high-entropy stabilised materials was initiated by Huang and Yeh in 1995 [1] by developing the high-entropy alloys (HEA) concept and was more recently extended to oxide materials (HEO) by Rost et al. [2]: single-phase multi-element oxide consisted of randomly distributed Co, Cu, Mg, Ni, Zn cations crystallised in a rock salt structure (Fm-3 m). The presence of several cations that can occupy the same crystallographic positions can lead to interesting physicochemical properties, and open up new possibilities for tailor-made functional materials [3]. High-entropy oxide materials with a spinel structure have been first studied by Dąbrowa et al. [4]. So far, several compositions, mainly based on transition metals, have been confirmed as single-phase high-entropy spinel oxides. Since the seminal work of Dąbrowa et al., following spinel compositions have been studied: $(Co,Cu,Fe,Mn,Ni)_3O_4$ [5], $(Cr,Fe,Mn,Ni,Zn,)_3O_4$ [6], $(Cr,Fe,Mn,Co,Ni,)_3O_4$ [4,6,7], $(Cr,Fe,Mn,Co,Zn)_3O_4$, $(Cr,Fe,Mg,Mn,Ni)_3O_4$, $(Co,Cr,Fe,Mg,Mn)_3O_4$ [8], $(Ni,Co,Mn,Fe,Ti)_3O_4$ [9], $(Mg,Ti,Zn,Cu,Fe)_3O_4$ [10].

The HEO research mainly focused on bulk materials (i.e. thick pellets obtained via high temperature solid state reaction methods), whereas the properties of the materials in the form of layers were only briefly reported [11]. Among the HEO spinel compounds discovered so far, $(Cr,Fe,Mn,Co,Ni,)_3O_4$ is one of the most studied compositions [12,13]. It is mainly produced by solid-state synthesis, however, there are several reports in the literature indicating the possibility of producing this material by chemical methods such as sol-gel [14] or solution combustion synthesis (SCS) [15]. The main disadvantage of conventional high-temperature methods is the high sintering temperature (900–1100 °C) and long isothermal holding (up to 24 h) required to obtain single-phase spinel oxide.

The selection of alternative synthesis methods can reduce time and annealing temperature. One such method is the spray pyrolysis deposition technique, which is widely used for the fabrication of thin films [16]. So far, spray-pyrolysis has been employed for the fabrication of stabilised zirconias [17,18], cerias [19,20], and spinels [21,22], but it has not been reported for the fabrication of multicomponent oxides described as high-entropy oxides. This technique involves atomizing precursor solutions into a fine mist or aerosol, which is then directed onto a heated substrate using a gas stream. The precursor solution is prepared by dissolving the desired materials, such as metal salts or

* Corresponding author at: Advanced Materials Center, Faculty of Electronics, Telecommunications and Informatics, Gdańsk University of Technology, ul. G. Narutowicza 11/12, 80-233 Gdańsk, Poland.
E-mail address: bartosz.kamecki@pg.edu.pl (B. Kamecki).

https://doi.org/10.1016/j.matchar.2023.113097
Received 7 March 2023; Received in revised form 26 May 2023; Accepted 11 June 2023
Available online 14 June 2023

organic compounds, in an appropriate solvent [23]. Given the wide availability of metal salts, this method offers a flexible fabrication platform, where multi-cation compositions can be readily fabricated. Atomization of the precursor solution can be achieved using various techniques, including pneumatic or ultrasonic nebulizers, pressure nozzles, or electrostatic sprayers [24]. The atomization process ensures the formation of a uniform and well-dispersed aerosol. Upon contact with the hot surface, the droplets undergo rapid thermal decomposition and chemical reactions. Volatile components evaporate, leaving behind solid particles that form, droplet by droplet, a thin film on the substrate. The temperature is carefully controlled to enable the desired chemical reactions and evaporation of the solvent, providing desired microstructure, while avoiding substrate damage or excessive thermal decomposition [25]. The deposition process is performed at low substrate temperatures (300–400 °C), at which either amorphous or partly crystalline materials can be deposited. By applying controlled post-deposition heat treatment, layers with different crystallinity and grain size can be obtained [26].

This work presents low-temperature spray-pyrolysis fabrication of HEO thin film and the determination of its basic properties. We report results concerning the structural and electrical properties of the (Mn,Co,Fe,Ni,Cr)$_3$O$_4$ composition on single-crystal sapphire Al_2O_3 and amorphous SiO_2 substrates.

2. Materials and methods

Fabrication of thin films was performed by an in-house-developed spray pyrolysis technique [27–29], which is based on the methodology developed by Prof. Gauckler's group [30]. Briefly, a liquid solution containing dissolved metal salts is atomised into droplets that are deposited on a heated substrate forming a deposit. A continuous layer is built drop-by-drop. The liquid precursor for the deposition process was prepared by mixing water-based solutions of the transition metal nitrates. Each nitrate was dissolved in distilled water (>12 MΩ cm^{-1}) to prepare individual solutions, which were then thermogravimetrically calibrated to determine the cation content. The calculated amounts and concentrations of cations per gram of nitrate aqueous solutions are provided below. The volume of the precursor solution was 50 ml and the total concentration of cations in the precursor solution was fixed at 0.2 mol L^{-1}. The composition of cations in the precursor solution was adjusted to achieve a final stoichiometry like ($Mn_{0.2}Co_{0.2}Fe_{0.2}Ni_{0.2}Cr_{0.2}$)$_3O_4$. Following nitrate solutions were used: 13611 g of 1.469 mmol/g Cr(NO$_3$)$_3$•9H$_2$O solution (Chempur, 97%), 14,554 g of 1374 mmol/g Mn(NO$_3$)$_2$• 4H$_2$O solution (Chempur, 98%), 12,922 g of 15,477 mmol/g Co(NO$_3$)$_2$ • 6H$_2$O solution (Chempur, 99%), 13,253 g of 15,091 mmol/g Fe(NO$_3$)$_3$ • 9H$_2$O solution (Chempur, 99%), and 13,162 g of 15,195 mmol/g Ni(NO$_3$)$_2$ • 6H$_2$O solution (Chempur, 98%). In the next step, an equimolar mixture of these nitrates dissolved in water was mixed with 50,625 g of tetraethylene glycol (Sigma-Aldrich, 99% purity) at a volume ratio of 1:9, respectively. Amorphous-SiO_2 (both sides polished, 10 × 10 × 0.2 mm^3, Continental Trade, Poland) and C-plane Sapphire (one side polished, 10 × 10 × 0.3 mm^3, CrysTec, Germany) substrates were placed on a hotplate and heated to 390 °C (controlled by a thermocouple placed below the sample). Deposition of a layer of ~500 nm thickness was achieved by using 5 ml of precursor fed at a rate of 2.5 ml min^{-1}, air atomised by an airbrush nozzle (Paasche VLS, USA). Post fabrication, the layers were thermally treated in a box furnace in the temperature range of 500–900 °C (ramping rate of 3 °C/min) for 20 h to evaluate the structural and microstructural features.

The microstructure of the samples was analysed by X-ray diffraction (XRD) using a Bruker D2 Phaser diffractometer with a Lynxeye XE-T detector with CuKα radiation (λ = 0.15406 nm) at room temperature.

The morphology of the samples on sapphire was investigated by scanning electron microscopy (FEI Quanta FEG 250) with an ET (Everhart–Thornley) secondary electron detector at an acceleration voltage of 20 kV. For elemental analysis, energy-dispersive x-ray spectroscopy (EDX) was performed by the EDAX Genesis APEX 2i software with an ApolloX SDD spectrometer.

TEM investigations were performed on high resolution on a Titan Cubed G2 60–300 (FEI) Probe Cs corrected (S)TEM equipped with a ChemiSTEM EDX detector system based on four windowless Silicon Drift Detectors (Super X). Visualisation of the extended crystal structure was performed in the VESTA software [31]. For TEM imaging, a HEO layer deposited on α-SiO_2 was annealed at 700 °C for 10 h and scraped off to obtain powder for analysis. A small amount of the powder was then diluted in high purity demineralised water. Next, the water containing the powder was put into an ultrasonic bath for about 5 min, then a drop of the water was transferred to a sample holder – a copper grid with a very thin carbon coating. In the following step, the sample was vacuum dried, and was then ready for TEM observation.

A sample deposited on the sapphire substrate was used for electrical characterisation by a four-wire van der Pauw method. The measurement was performed utilising a custom-built rig based on a Keithley 2400 SourceMeter and a multiplexer. The sample was contacted at the corners by Pt wires attached by silver paste. The multiplexer changes the electrodes as required by the van der Pauw technique. The temperature was controlled by a PID controller contacted with the thermocouple placed directly above the sample surface. The measurement was performed in sequential temperature ramps. After each longer dwell (2 h), starting from 500 °C, the temperature was lowered in steps by 50 °C (3 °C/min) and held for 30 min at each temperature. After reaching 300 °C, the temperature was increased to reach temperature 100 °C higher than the previous maximum temperature.

3. Results and discussion

The deposited layers were measured after deposition and after post-annealing for 20 h at 500, 600, 700, 800, and 900 °C. Fig. 1 presents the XRD patterns of layers deposited on α-SiO_2 (A) and SEM surface images of an as-deposited layer (B). Irrespective of the substrate type, both as-deposited layers were crack-free and the surface looks as presented in Fig. 1B. Rings due to splashed droplets, typical for the spray deposition method, are visible on the surface.

No peaks related to crystal structure could be noticed in the XRD pattern for the as-deposited layer (~400 °C). The diffraction spectrum shows only the background signal of the amorphous silica (α-SiO_2) substrate with a characteristic bump in the low angle range. The diffraction peaks were revealed after annealing layers at 500 °C, indicating crystallisation of the layer upon heat treatment. All of the observed peaks can be attributed to a face-centred cubic single-phase spinel structure (Fd-3 m) described by space group no. 227 (ICDD PDF no. 01–077-0008). For the 500 and 600 °C annealing temperatures, reflections were quite broad with low intensity. The less intense peaks corresponding to the (111), (222), and (422) planes were not visible, indicating low crystallisation. Layers annealed above 600 °C showed spectra of a well-crystallised material. We have previously shown that the spray pyrolysis layers contain leftover C—O groups after deposition and annealing up to 600 °C, and after their removal full crystallisation of the deposited films occurs [32]. Le Bail refinement was used to calculate the lattice parameter of the produced layers, as well as the crystallite size, which was calculated according to the Scherrer equation (k taken as 0.89) [33]. Comparison of the temperature dependence on the structural features is summarised in Table 1, and detailed refinement data is attached in the supplementary section in Tables S1–S5. The heat treatment did not induce a significant change of the lattice constant. The obtained values of the lattice constant are comparable with the results of Mao et al. [15]. Other groups using the conventional solid-state synthesis route report a higher lattice parameter of 8.33–8.35 [8,34,35]. Depending on the thermal history, spinels can show different oxidation states of the transition metal elements, thus influencing the lattice parameter [36,37]. The crystallite dimensions increased from ~26 nm to ~109 nm with the increasing annealing temperature, which is typical

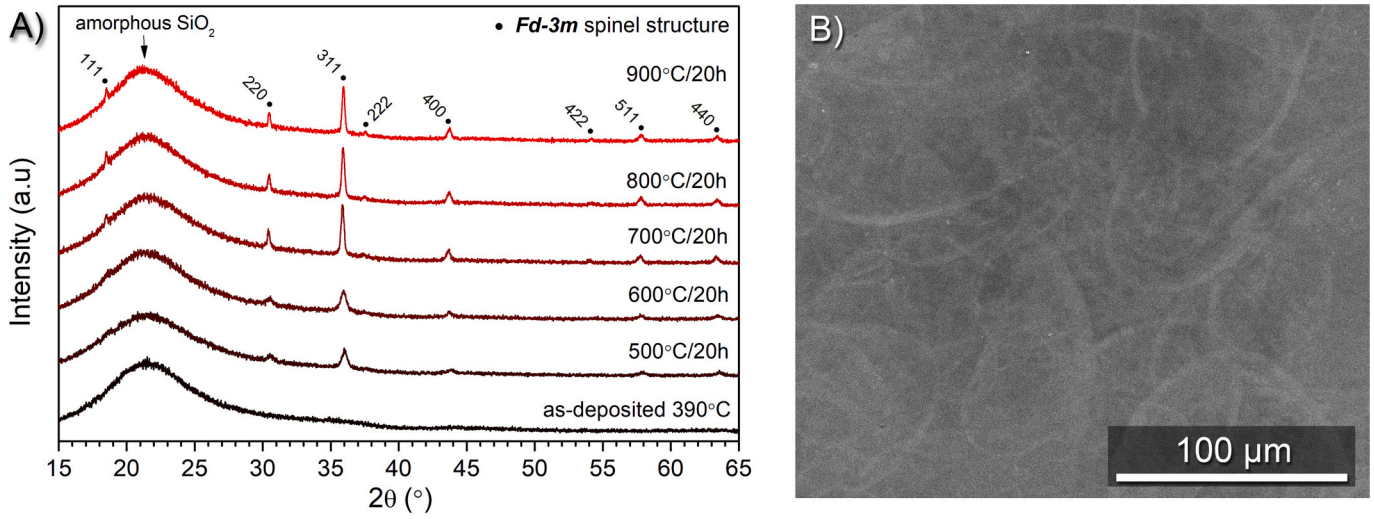

Fig. 1. A) XRD Patterns of $(Cr,Fe,Mn,Co,Ni,)_3O_4$ layers deposited on α-SiO_2 substrate and annealed at different temperatures, B) SEM surface image of an as-deposited layer on α-SiO_2 substrate.

Table 1
Crystal structure parameters, calculated grain size from SEM images and EDX chemical composition results.

	Structural parameters			Chemical composition [± 2%]				
Annealing temperature (°C)	*a* lattice parameter (Å)	Crystallite size (nm)	Grain size (nm)	Cr	Mn	Fe	Co	Ni
500	8.280	26	28	18	19	19	21	22
600	8.285	23	29	19	18	19	21	22
700	8.295	59	77	18	20	19	21	22
800	8.286	70	129	18	19	20	21	22
900	8.283	109	216	15	19	21	22	23

for thin films processed via spray-pyrolysis [32]. The nanocrystalline (crystallite size <100 nm) state of the layer could be retained for temperatures below 900 °C.

The energy-dispersive x-ray spectroscopy results are presented in Fig. 2. The distribution of the elements was uniform throughout the sample surface, with no traces of agglomeration. On the EDX maps shown in Fig. 2A, slight differences in intensity can be noticed, which are associated with the presence of unevenness on the surface of the layer. In places where the layer is thinner, the signal of the α-SiO2 substrate is more intense than that of the transition metals present in the layer. Slight differences result from the existing surface roughness resulting from the overlapping of droplets in the deposition process. The liquid precursors used for layer preparation, with cations well mixed at a molecular level, can facilitate the formation of homogeneous materials. Elemental composition (at. %) was calculated from the low magnitude SEM surface images (integrated over large area) and summarised in Table 1 as well as presented in the form of EDX spectra in Fig. 2B. The obtained results proved the equimolar ratio of the cations in the produced samples. A slightly higher concentration of Co and Ni could be observed, which is still within the limits of measurement uncertainty. Moreover, the sample annealed at 900 °C revealed a significant decrease in Cr content, which suggests evaporation of volatile chromium compounds over 800 °C, possibly due to high pO_2 (air) and the expected level of humidity.

SEM surface and fracture cross-section images of samples annealed at three different temperatures (500, 700, 900 °C) are presented in Fig. 3. Regardless of the annealing temperature, samples showed a dense, uniform microstructure consisting of nano-dimensioned grains with thickness in a range of 400–500 nm. According to the crystallite-size calculations presented in Table 1, the grain dimensions revealed the

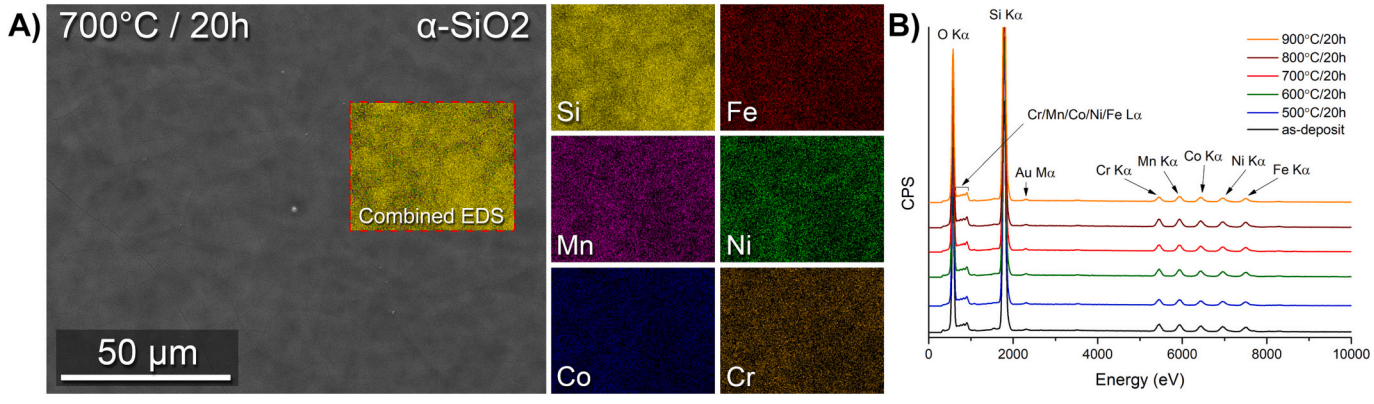

Fig. 2. A) EDX maps of HEO layer deposited on α-SiO_2 and annealed at 700 °C in 20 h, B) EDX spectra of samples annealed at different temperatures.

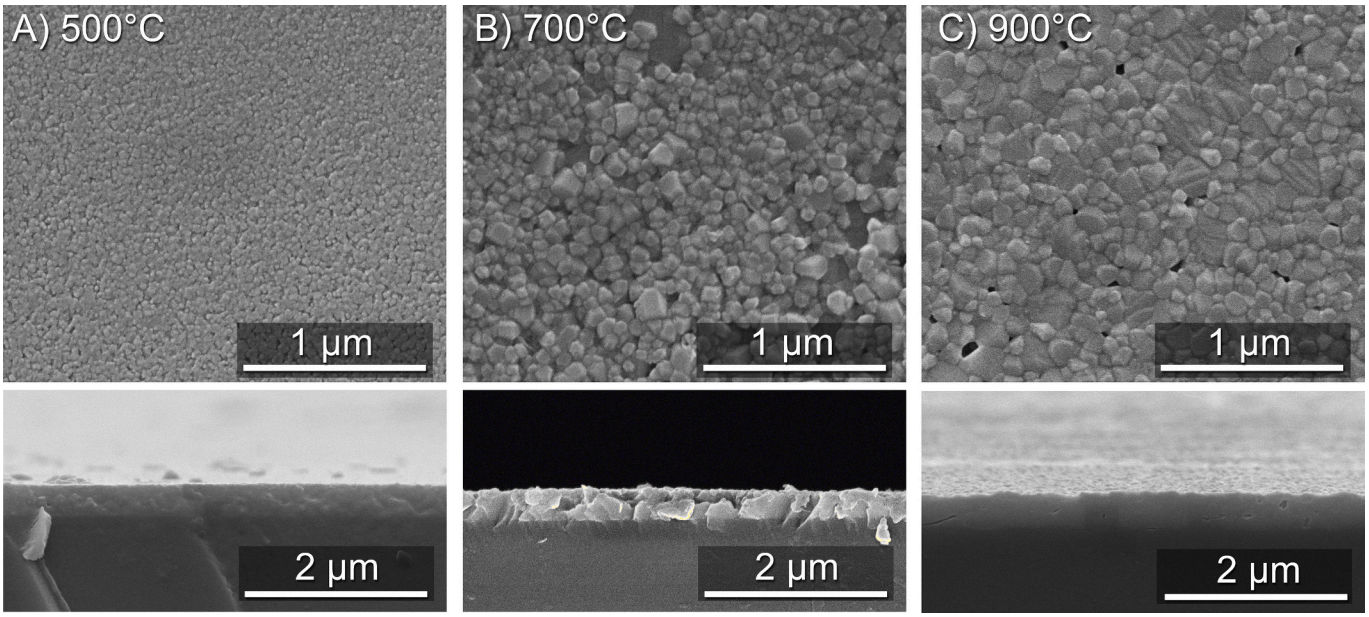

Fig. 3. Surface and cross-section SEM images of HEO layers on α-SiO_2 annealed at A) 500 °C, B) 700 °C, and C) 900 °C.

same correlation of size change with increasing annealing temperature. Differences in surface morphology are visible between samples annealed at different temperature ranges.

Transmission Electron Microscopy (TEM) analysis was performed to characterise the crystal structure and determine the elemental distribution at the nanoscale. The STEM-EDX maps presented in Fig. 4G proved that the composition and distribution of the elements are homogeneous at the level of single particles. There was no agglomeration or secondary phase formation detectable during the TEM analysis. The HAADF-STEM image in Fig. 4C presents a high-resolution image of the spinel, with a particular arrangement of atoms. The arrangement presented in Fig. 4C corresponds to a view along the (Zone axis 112) direction, as confirmed by comparison with theoretical prediction, confirming a cubic spinel structure. In Fig. 4D and E SAED patterns are presented with simulated spinel structure in (112) direction to verify the face centered cubic (FCC) structure. These results confirmed the possibility of deposition of elementally homogeneous, singe-phase high-quality ~500 nm layers of HEO spinels using the spray pyrolysis

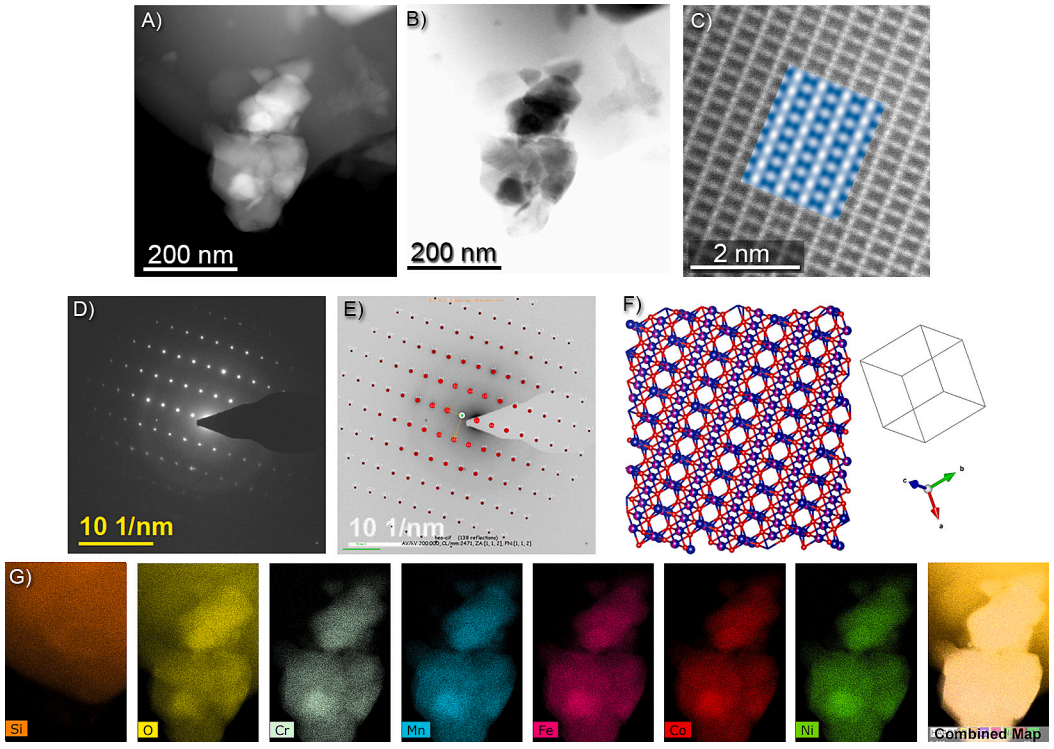

Fig. 4. A), B) STEM and BF-STEM image of HEO annealed at 700 °C, C) HAADF-STEM image with simulated spinel structure in (112) direction D), E) SAED patterns with simulated spinel structure in (112) direction, F) Extended crystal structure simulation projected along (112) vector, G) STEM-EDX chemical composition maps of the individual components and the combined map.

method.

HEO layers deposited on α-SiO_2 start cracking after heat-treatment above 600 °C. The STEM-EDX chemical composition maps presented in Fig. 4G did not reveal the presence of Si in the HEO grains, therefore the layer cracking is possibly due to a mismatch of the thermal expansion coefficient (TEC) as opposed to a reaction with the Si present in the substrate. Stygar et al. reported a TEC for $(Mn_{0.2}Co_{0.2}Fe_{0.2}Ni_{0.2}Cr_{0.2})_3O_4$ of 9.7 • 10^{-6} K^{-1} [7]. Based on the substrate supplier's technical datasheets, the thermal expansion coefficients are 5.5 • 10^{-7} K^{-1} (@ 20–320 °C) and 5–6.66 • 10^{-6} K^{-1} (@ 50 °C) for α-SiO_2 and Sapphire, respectively. It shows that the sapphire TEC is closer to the spinel TEC value than amorphous silica. Due to the cracking of the layer deposited on α-SiO_2, the electrical measurement could not be carried out on this substrate. Therefore electrical characterisation was performed on the HEO layer deposited on Sapphire. Additional characterisation of layers deposited on the sapphire substrate was performed and the results are plotted and summarised in the supplementary materials.

The electrical conductivity study was performed on an as-deposited sample that was subjected to a measurement procedure that included steps with increasing temperature. Five cycles were performed; each subsequent cycle was higher by 100 °C than the previous one in the range of 500–900 °C. The conductivity used for the Arrhenius plot presented in Fig. 5 was examined during cooling down in temperature steps of 50 °C. The amorphous samples showed a very low level of electrical conductivity, below the measurement limit, thus the results from the higher temperatures (after dwell at 500 °C) are presented. Fig. 5 shows the Arrhenius-type plot of electrical conductivity as a function of temperature. The observed temperature behaviour of the electrical conductivity indicates thermally activated conductivity. The activation energy for the measured sample has a different slope for the high temperature (HT) and low temperature (LT) regimes correlated with a possible change of the conduction mechanism, caused possibly by a change from grain-boundary to grain dominated electrical transport, or, alternatively, to thermal oxidation of some of the spinel component. The inflection point of the conductivities is below 600 °C and is around ~150 °C higher than 394 °C previously reported by Stygar et al. for the same material composition however, synthesized utilising solid-state reaction [7]. Activation energies reported by Stygar group were 0.31 eV and 0.61 eV at the low and high-temperature range, respectively. Values obtained in this research for the same material composition, but deposited in form of the nanocrystalline film were lower and equal to 0.20 eV and 0.27 eV at the low and high-temperature range, respectively.

Fig. S5 presents the measured electrical conductivity as a function of the maximum exposure temperature. According to the legend, symbols connected with line obtained at the same measurement temperature compare results measured after exposing the sample on different annealing temperature. The data presented in this way indicates that the optimal annealing temperature to maximize the electrical performance is 700 °C. Obtained values of total conductivity measured at 700 °C equaled 3; 2.2 and 0.9 S•cm^{-1} for sample exposed at 700, 800 and 900 °C, respectively. Annealing the material at higher temperatures resulted in a decrease of the maximum total conductivity values for the 800 and 900 °C temperatures, probably due to Cr evaporation what was confirmed by EDX. Lower values of electrical conductivity for samples annealed below 700 °C were caused by insufficient crystallisation of the layer, as proven by the structural investigations presented above.

4. Conclusions

High-entropy spinel oxide with a composition of (Mn,Co,Fe,Ni,Cr)$_3O_4$ was successfully deposited as a nanocrystalline, ~500 nm thin film using the spray pyrolysis technique. Phase-pure cubic spinels with homogeneously distributed elements were obtained at low temperatures (crystallisation at 500 °C). The electrical conductivity of the spinels was studied at high temperatures and showed a maximum value of ~3 S

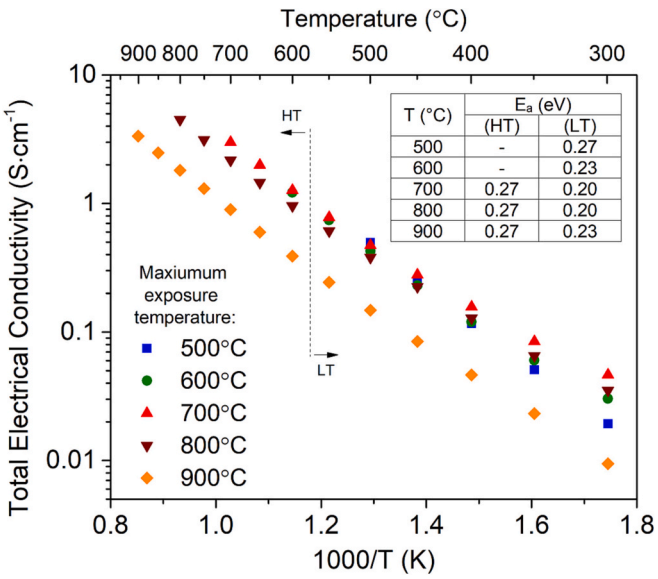

Fig. 5. Total electrical conductivity measured using Van der Pauw method. Arrhenius-type plot of Electrical conductivity as a function of temperature.

cm^{-1} at 700 °C (for the layer heat-treated at 700 °C). Previous work in this area is related mainly to the structural properties of bulk materials, fabricated by solid-state syntheses and having large particles. The research conducted on nanocrystalline thin layers with controlled grain size is, therefore, an interesting development of existing research and expands the knowledge of the production of HEOs in the form of nanomaterials.

Declaration of Competing Interest

The authors declare that they have no known competing financial interests or personal relationships that could have appeared to influence the work reported in this paper.

Data availability

Data will be made available on request.

Acknowledgements

This research has been supported by National Science Centre (NCN) Miniatura 2 project number 2018/02/X/ST5/01878: "Preparation and characterization of multicomponent oxides in the form of thin films" and Preludium 18 project number 2019/35/N/ST5/01796: "Nanocrystalline high-entropy spinel oxide films: the influence of electron configuration and crystallographic position of cations on physicochemical properties".

Appendix A. Supplementary data

Supplementary data to this article can be found online at https://doi.org/10.1016/j.matchar.2023.113097.

References

[1] J.Y.K.H. Huang, A Study on the Multicomponent Alloy Systems Containing Equal-Mole Elements, National Tsing Hua University, 1996.
[2] C.M. Rost, E. Sachet, T. Borman, A. Moballegh, E.C. Dickey, D. Hou, J.L. Jones, S. Curtarolo, J.P. Maria, Entropy-stabilized oxides, Nat. Commun. 6 (2015), https://doi.org/10.1038/ncomms9485.
[3] A. Sarkar, B. Breitung, H. Hahn, High entropy oxides: the role of entropy, enthalpy and synergy, Scr. Mater. 187 (2020) 43–48, https://doi.org/10.1016/j.scriptamat.2020.05.019.
[4] J. Dąbrowa, M. Stygar, A. Mikuła, A. Knapik, K. Mroczka, W. Tejchman, M. Danielewski, M. Martin, Synthesis and microstructure of the (Co,Cr,Fe,Mn,Ni)

3O4 high entropy oxide characterized by spinel structure, Mater. Lett. 216 (2018) 32–36, https://doi.org/10.1016/j.matlet.2017.12.148.
[5] S. Wang, Dongdong Wang, Z. Liu, S. Du, Y. Zhang, H. Li, R. Chen, Y. Wang, Yuqin Zou, Z. Xiao, W. Chen, Low-temperature synthesis of small-size high-entropy oxide for water oxidation, J. Mater. Chem. A (2019) 24211–24216, https://doi.org/10.1039/c9ta08740k.
[6] A. Mao, H.-Z. Xiang, Z.-G. Zhang, K. Kuramoto, H. Zhang, Y. Jia, A new class of spinel high-entropy oxides with controllable magnetic properties, J. Magn. Magn. Mater. 497 (2019), 165884, https://doi.org/10.1016/j.jmmm.2019.165884.
[7] M. Stygar, J. Dąbrowa, M. Moździerz, M. Zajusz, W. Skubida, Journal of the European Ceramic Society Formation and properties of high entropy oxides in Co-Cr-Fe-Mg-Mn-Ni-O system : Novel (Cr , Fe , Mg , Mn , Ni) 3 O 4 and (Co , Cr , Fe , Mg , Mn) 3 O 4 high entropy spinels, J. Eur. Ceram. Soc. (2019) 1–7, https://doi.org/10.1016/j.jeurceramsoc.2019.11.030.
[8] Z. Grzesik, G. Smo, M. Stygar, M. Zajusz, K. Mroczka, M. Danielewski, Journal of the European Ceramic Society Defect structure and transport properties in (Co , Cu , Mg , Ni , Zn) O high entropy oxide 39 (2019) 4292–4298, https://doi.org/10.1016/j.jeurceramsoc.2019.06.018.
[9] T.Y. Chen, S.Y. Wang, C.H. Kuo, S.C. Huang, M.H. Lin, C.H. Li, H.Y.T. Chen, C. C. Wang, Y.F. Liao, C.C. Lin, Y.M. Chang, J.W. Yeh, S.J. Lin, T.Y. Chen, H.Y. Chen, In operando synchrotron X-ray studies of a novel spinel (Ni0.2Co0.2Mn0.2Fe0.2Ti0.2)3O4high-entropy oxide for energy storage applications, J. Mater. Chem. A 8 (2020) 21756–21770, https://doi.org/10.1039/d0ta06455f.
[10] H. Chen, N. Qiu, B. Wu, Z. Yang, S. Sun, Y. Wang, A new spinel high-entropy oxide (Mg0.2Ti0.2Zn0.2Cu0.2Fe0.2)3O4 with fast reaction kinetics and excellent stability as an anode material for lithium ion batteries, Crystals. 10 (2021) 9736–9744, https://doi.org/10.1039/d0ra00255k.
[11] T.X. Nguyen, Y.H. Su, J. Hattrick-Simpers, H. Joress, T. Nagata, K.S. Chang, S. Sarker, A. Mehta, J.M. Ting, Exploring the first high-entropy thin film libraries: composition spread-controlled crystalline structure, ACS Comb. Sci. 22 (2020) 858–866, https://doi.org/10.1021/acscombsci.0c00159.
[12] C.-C. Lin, C.-W. Chang, C.-C. Kaun, Y.-H. Su, Stepwise evolution of photocatalytic spinel-structured (Co,Cr,Fe,Mn,Ni)3O4 high entropy oxides from first-principles calculations to machine learning, Crystals. 11 (2021) 1035, https://doi.org/10.3390/cryst11091035.
[13] A. Mao, H.Z. Xiang, Z.G. Zhang, K. Kuramoto, H. Zhang, Y. Jia, A new class of spinel high-entropy oxides with controllable magnetic properties, J. Magn. Magn. Mater. 497 (2020) 1–5, https://doi.org/10.1016/j.jmmm.2019.165884.
[14] G. Wang, J. Qin, Y. Feng, B. Feng, S. Yang, Z. Wang, Y. Zhao, J. Wei, Sol-gel synthesis of spherical mesoporous high-entropy oxides, ACS Appl. Mater. Interfaces 12 (2020) 45155–45164, https://doi.org/10.1021/acsami.0c11899.
[15] A. Mao, F. Quan, H.Z. Xiang, Z.G. Zhang, K. Kuramoto, A.L. Xia, Facile synthesis and ferrimagnetic property of spinel (CoCrFeMnNi)3O4 high-entropy oxide nanocrystalline powder, J. Mol. Struct. 1194 (2019) 11–18, https://doi.org/10.1016/j.molstruc.2019.05.073.
[16] S. Molin, A. Chrzan, J. Karczewski, D. Szymczewska, P. Jasinski, The role of thin functional layers in solid oxide fuel cells, Electrochim. Acta 204 (2016) 136–145, https://doi.org/10.1016/j.electacta.2016.04.075.
[17] B. Scherrer, S. Heiroth, R. Hafner, J. Martynczuk, A. Bieberle-Hütter, J.L.M. Rupp, L.J. Gauckler, Crystallization and microstructure of yttria-stabilized-zirconia thin films deposited by spray pyrolysis, Adv. Funct. Mater. 21 (2011) 3967–3975, https://doi.org/10.1002/adfm.201101268.
[18] D. Stender, R. Frison, K. Conder, J.L.M. Rupp, B. Scherrer, J.M. Martynczuk, L. J. Gauckler, C.W. Schneider, T. Lippert, A. Wokaun, Crystallization of zirconia based thin films, Phys. Chem. Chem. Phys. 17 (2015) 18613–18620, https://doi.org/10.1039/c5cp02631h.
[19] J.L.M. Rupp, A. Infortuna, L.J. Gauckler, Microstrain and self-limited grain growth in nanocrystalline ceria ceramics, Acta Mater. 54 (2006) 1721–1730, https://doi.org/10.1016/j.actamat.2005.11.032.
[20] L. dos Santos-Gómez, J. Zamudio-García, J.M. Porras-Vázquez, E.R. Losilla, D. Marrero-López, Highly oriented and fully dense CGO films prepared by spray-pyrolysis and different precursor salts, J. Eur. Ceram. Soc. 40 (2020) 3080–3088, https://doi.org/10.1016/j.jeurceramsoc.2020.03.026.
[21] D. Szymczewska, S. Molin, P. Hendriksen, P. Jasiński, Microstructure and electrical properties of Fe,Cu substituted (Co,Mn)3O4 thin films, Crystals. (2017), https://doi.org/10.3390/cryst7070185.
[22] L.D. Conceicao, E. Djurado, L. Dessemond, E.N.S. Muccillo, Fabrication of Mn1.5Co1.5O4 by electrostatic spray deposition for application as protective coating on alloy interconnects for solid oxide fuel cells, ECS Trans. 68 (2015) 1609–1616, https://doi.org/10.1149/06801.1609ecst.
[23] D. Perednis, L.J. Gauckler, Thin film deposition using spray pyrolysis, J. Electroceram. 14 (2005) 103–111.
[24] D. Beckel, A. Bieberle-Hütter, A. Harvey, A. Infortuna, U.P. Muecke, M. Prestat, J.L. M. Rupp, L.J. Gauckler, Thin films for micro solid oxide fuel cells, J. Power Sources 173 (2007) 325–345, https://doi.org/10.1016/j.jpowsour.2007.04.070.
[25] U.P. Muecke, N. Luechinger, L. Schlagenhauf, L.J. Gauckler, Initial stages of deposition and film formation during spray pyrolysis - nickel oxide, cerium gadolinium oxide and mixtures thereof, Thin Solid Films 517 (2009) 1522–1529, https://doi.org/10.1016/j.tsf.2008.08.115.
[26] B. Scherrer, A. Rossi, J. Martynczuk, M.D. Rossell, A. Bieberle-Hütter, J.L.M. Rupp, R. Erni, L.J. Gauckler, Impact of substrate material and annealing conditions on the microstructure and chemistry of yttria-stabilized-zirconia thin films, J. Power Sources 196 (2011) 7372–7382, https://doi.org/10.1016/j.jpowsour.2011.03.077.
[27] B. Kamecki, J. Karczewski, P. Jasiński, S. Molin, Improvement of oxygen electrode performance of intermediate temperature solid oxide cells by spray pyrolysis deposited active layers, Adv. Mater. Interfaces 2002227 (2021) 1–11, https://doi.org/10.1002/admi.202002227.
[28] B. Kamecki, J. Karczewski, T. Miruszewski, G. Jasiński, D. Szymczewska, P. Jasiński, S. Molin, Low temperature deposition of dense MnCo2O4protective coatings for steel interconnects of solid oxide cells, J. Eur. Ceram. Soc. 38 (2018) 4576–4579, https://doi.org/10.1016/j.jeurceramsoc.2018.05.042.
[29] B. Kamecki, J. Karczewski, P. Jasiński, S. Molin, Evaluation of praseodymium and gadolinium doped ceria as a possible barrier layer material for solid oxide cells, ECS Trans. 91 (2019) 1165–1172, https://doi.org/10.1149/09101.1165ecst.
[30] D. Perednis, Thin film deposition by spray pyrolysis and the application in solid oxide fuel cells, ETH Zürich (2003), https://doi.org/10.3929/ethz-a-004637544.
[31] K. Momma, F. Izumi, VESTA: a three-dimensional visualization system for electronic and structural analysis, J. Appl. Crystallogr. (2008), https://doi.org/10.1107/S0021889808012016.
[32] B. Kamecki, J. Karczewski, H. Abdoli, M. Chen, G. Jasiński, P. Jasiński, S. Molin, Deposition and electrical and structural properties of La0.6Sr0.4CoO3 thin films for application in high-temperature electrochemical cells, J. Electron. Mater. 48 (2019) 5428–5441, https://doi.org/10.1007/s11664-019-07372-7.
[33] A.L. Patterson, The scherrer formula for X-ray particle size determination, Phys. Rev. 56 (1939) 978–982, https://doi.org/10.1103/PhysRev.56.978.
[34] D. Wang, S. Jiang, C. Duan, J. Mao, Y. Dong, K. Dong, Z. Wang, S. Luo, Y. Liu, X. Qi, Spinel-structured high entropy oxide (FeCoNiCrMn)3O4 as anode towards superior lithium storage performance, J. Alloys Compd. 844 (2020), 156158, https://doi.org/10.1016/j.jallcom.2020.156158.
[35] J. Dąbrowa, M. Stygar, A. Mikuła, A. Knapik, K. Mroczka, W. Tejchman, M. Danielewski, M. Martin, Synthesis and microstructure of the (Co,Cr,Fe,Mn,Ni) 3O4high entropy oxide characterized by spinel structure, Mater. Lett. 216 (2018) 32–36, https://doi.org/10.1016/j.matlet.2017.12.148.
[36] B. Talic, P.V. Hendriksen, K. Wiik, H.L. Lein, Thermal expansion and electrical conductivity of Fe and cu doped MnCo2O4spinel, Solid State Ionics 326 (2018) 90–99, https://doi.org/10.1016/j.ssi.2018.09.018.
[37] C. Wei, Z. Feng, G.G. Scherer, J. Barber, Y. Shao-Horn, Z.J. Xu, Cations in octahedral sites: a descriptor for oxygen Electrocatalysis on transition-metal Spinels, Adv. Mater. 29 (2017), https://doi.org/10.1002/adma.201606800.